THE JOURNAL OF PHYSICAL CHEMISTRY C

Article

pubs.acs.org/JPCC

Surface-Induced Anisotropic Binding of a Rhenium CO_2-Reduction Catalyst on Rutile TiO_2(110) Surfaces

Aimin Ge,[†,∥] Benjamin Rudshteyn,[‡,§,∥] Brian T. Psciuk,[‡] Dequan Xiao,[‡,§,⊥] Jia Song,[†] Chantelle L. Anfuso,[†,#] Allen M. Ricks,[†] Victor S. Batista,[*,‡,§] and Tianquan Lian[*,†]

[†]Department of Chemistry, Emory University, Atlanta, Georgia 30322, United States

[‡]Department of Chemistry, Yale University, New Haven, Connecticut 06520, United States

[§]Yale Energy Sciences Institute, Yale University, West Haven, Connecticut 06516, United States

Supporting Information

ABSTRACT: Vibrational sum frequency generation (SFG) spectroscopy has been utilized to study the spatial orientation and alignment of $Re(CO)_3Cl$(dcbpy) (dcbpy = 4,4′-dicarboxy-2,2′-bipyridine) (or ReC0A) on the (001) and (110) surfaces of rutile single-crystalline TiO_2. The SFG intensity of the CO stretching modes shows an isotropic distribution on the (001) surface and an anisotropic distribution on the (110) surfaces with respect to the in-plane rotation of the crystal relative to the surface normal (or the incident laser beam plane). By combining these results with ab initio SFG simulations and with modeling of ReC0A−TiO_2 cluster binding structures at the density functional theory level, we reveal that the origin of the optical anisotropy for ReC0A on the TiO_2(110) surface is associated with the binding preference of ReC0A along the [−110] axis. Along this direction, the binding structure is energetically favorable, because of the formation of proper hydrogen bonding between the carboxylate group and passivating water molecules adsorbed on the TiO_2(110) surface. Simulations of dimers of ReC0A molecules binding close together with full nearest-neighbor effects give a structure that reproduces the experimental SFG polar plot. The tilt angle, defined by the bpy ring angle relative to the surface normal, of the catalyst is found to be 26° for one monomer and 18° for the other, which corresponds to an aggregate at high surface coverage.

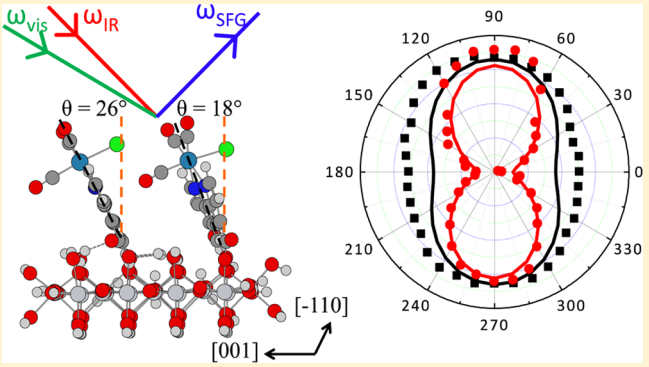

1. INTRODUCTION

The performance of photocatalytic and electrocatalytic systems is often highly dependent on the microscopic ordering of catalytic molecules on a scaffolding support system.[1−4] The molecule−semiconductor electrode interface is of particular interest because of its relevance in many types of catalytic systems.[5−11] Because molecular orientation in these systems can significantly influence their catalytic performance, the ability to control the molecular ordering through careful selection of the surface structure and symmetry would be extremely beneficial. An investigation of catalytic molecules on surfaces with different symmetries may elucidate how the degree of molecular ordering depends on surface structure and therefore is of great practical interest.

Vibrational sum frequency generation (SFG) spectroscopy has been recognized in recent years as a useful technique for determining average molecular conformation at interfaces.[12−14] As a second-order optical technique, it is forbidden in media with inversion symmetry, but is allowed at interfaces where inversion symmetry is necessarily broken.[15] SFG is thus surface-specific, giving it a distinct advantage over other optical techniques and making it an ideal tool for elucidating a molecular-level picture of structure and dynamics for molecule−semiconductor as well as molecule−metal systems.[16−19] Although it is typically used to determine the average molecular tilt angle for molecules on isotropic surfaces, it can also be used to determine the degree of anisotropy in these interfacial systems. Specifically, by monitoring the molecular sum frequency response as a function of the surface azimuthal angle, the anisotropic orientation distribution can be deduced.[20−26]

$Re(CO)_3Cl$(dcbpy) (dcbpy = 4,4′-dicarboxy-2,2′-bipyridine) (or ReC0A) and several derivatives have been explored in recent years for catalytic reduction of CO_2 to CO.[4,27−34] Binding of a rhenium bipyridyl complex to TiO_2 electrodes has also been shown to increase catalytic reductive ability.[9] Characterizing the ReC0A/TiO_2 interface is thus important to fully understand this important catalytic system. Previously, we investigated the orientation of ReC0A on the single-crystalline TiO_2(001) surface using a combination of vibrational SFG spectroscopy

Special Issue: Richard P. Van Duyne Festschrift

Received: March 28, 2016
Revised: May 31, 2016
Published: May 31, 2016

DOI: 10.1021/acs.jpcc.6b03165
J. Phys. Chem. C 2016, 120, 20970−20977

Scheme 1. (a) Energy Level Diagram for a SFG Process; (b) Schematic of the SFG Setup with *ppp* Polarization Combination;[a] (c) Schematic Illustration of the Orientation Angles Used to Model the ReC0A Complex Dimer on the TiO_2 Rutile (110) Surface[b]

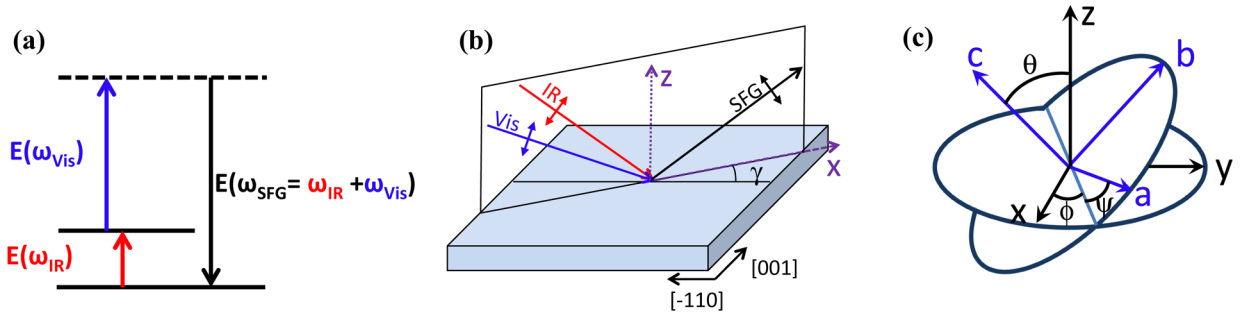

[a]The laser beams are in the *xz* plane of the laboratory coordinate system. γ is the orientation angle of TiO_2(110) single crystal, defined as the angle between the [−110] crystal axis and *x*-axis. [b]Axes *x*, *y*, and *z* represent the laboratory coordinate of the TiO_2 surface, while *a*, *b*, and *c* represent the molecular coordinates of the ReC0A complex in the theoretical model. Orientation angles θ, ψ, and ϕ are the Euler transformation angles between the two Cartesian coordinates in the *ZXZ* rotation matrix formalism.

and density functional theory (DFT) calculations and found that the complex oriented roughly normal to the TiO_2 surface.[35] In this work, we examine whether the adsorption geometry is controlled by the surface symmetry of the substrate by comparing the azimuthal angle dependences of the SFG intensity on the isotropic (001) and anisotropic (110) surfaces. We show that ReC0A has a well-defined anisotropic arrangement following the C_{2v} symmetry of the TiO_2(110) surface, in contrast to an isotropic distribution on the C_{4v} symmetric TiO_2(001) surface. We use ab initio SFG simulations to reveal the origin of the anisotropic SFG signals, which is further verified by modeling the binding geometry of ReC0A along different directions on the TiO_2(110) surface.

2. EXPERIMENTAL AND COMPUTATIONAL METHODS

2.1. Sample Preparation. Rutile (001) and (110) crystals were purchased from Commercial Crystal Laboratories, Inc. The crystals were cleaned and sensitized according to published procedures.[35,36] Briefly, the crystals were first sonicated in piranha solution (3:1 H_2SO_4/H_2O_2) for 1 h, followed by a Milli-Q (18 MΩ·cm) water rinse. They were placed in 1 M NaOH solution for 5 min, followed by another Milli-Q rinse. The crystals were then exposed to ultraviolet (UV) radiation for 10 min in 1 M HCl bath. After the UV treatment, the crystals were rinsed with ethanol and immediately immersed in 1 mM ReC0A/ethanol solution. The TiO_2 crystals were sensitized for 1 day and then washed with ethanol to remove any weakly adsorbed molecules prior to use. The samples were stored in a dark and dry environment to preserve sample integrity. The morphology of the surface was examined by atomic force microscopy (Figure S1 in the Supporting Information).

2.2. Sum Frequency Generation Spectroscopy. The broadband vibrational SFG setup is based on a 1 kHz Spitfire Ti:sapphire regenerative amplifier system (Spectra Physics) producing 150 fs pulses at 800 nm with a pulse energy of 4 mJ. Half of the fundamental was used to pump a TOPAS-C OPA (Light Conversion) producing tunable infrared (IR) pulses with energies of 10−15 μJ and a bandwidth of ∼150 cm^{-1}. The remaining 2 mJ of 800 nm output is spectrally narrowed to ∼10 cm^{-1} by using a home-built pulse shaper. The visible pulses were filtered to 2 μJ/pulse and combined with the IR at the sample surface. The angles of incidence of visible and IR are 65° and 50° with respect to the surface normal, respectively. The sample was mounted on a rotation stage to monitor the SFG signal as a function of azimuthal angle (γ) of TiO_2 single crystal. The reflected sum frequency signal was collimated and refocused onto the slit of a 300 mm monochromator (Acton Spectra-Pro 300i) and detected with a liquid nitrogen-cooled CCD (Princeton Instruments, PyLoN, 1340 × 100 pixels) operating at −120 °C. The SFG signal from the sample surface was focused onto four pixel stripes in the vertical direction. The acquisition time for each SFG spectrum is between 1 and 3 min. All spectra were collected under the *ppp* polarization combination (*p*-polarized SFG, *p*-polarized visible, *p*-polarized IR) and normalized by the SFG spectra of gold thin film measured under the same conditions.

In general, the vibrational SFG intensity from a sample can be expressed as[37]

$$I_{\mathrm{SFG}} \propto |\chi^{(2)}_{\mathrm{NR,eff}} + \chi^{(2)}_{\mathrm{R,eff}}|^2 = \left| A_{\mathrm{NR,eff}} e^{i\delta} + \sum_q \frac{A_{q,\mathrm{eff}}}{\omega_{\mathrm{IR}} - \omega_q + i\Gamma_q} \right|^2 \quad (1)$$

$\chi^{(2)}_{\mathrm{R,eff}}$ and $\chi^{(2)}_{\mathrm{NR,eff}}$ are the effective resonant and nonresonant nonlinear susceptibility tensors, respectively, which are products of susceptibility tensor elements and Fresnel coefficients. As shown in eq 1, $\chi^{(2)}_{\mathrm{R,eff}}$ can be approximated as a sum of Lorentzian functions, where $A_{q,\mathrm{eff}}$, ω_q, and Γ_q are the effective amplitude, frequency, and damping constant, respectively, of the *q*th SFG active vibrational mode and ω_{IR} is the frequency of the incident tunable infrared beam. Additionally, eq 1 shows that $\chi^{(2)}_{\mathrm{NR,eff}}$ has contributions from both $A_{\mathrm{NR,eff}}$ and δ, which are the effective amplitude and phase, respectively, of the nonresonant response.

2.3. Computational Methods. A slab of rutile (110) TiO_2 was optimized with periodic boundary conditions as implemented in the SIESTA software package.[38] The TiO_2(110) slab was represented by a three-dimensional periodic slab with at least 15 Å of vacuum in the vertical direction to eliminate interactions between the top of the system and the periodic image of the bulk TiO_2. The Perdew−Burke−Ernserhof generalized gradient approximation density functional was used to describe electron exchange and correlation.[39,40] A gamma point sampling (single k-point) was used as well as a 200 Ry cutoff for the plane-wave basis. The default convergence criteria were used for both the electronic energy and nuclear geometry optimizations.

The slab was then cut to a small cluster model with 16 TiO_2 units. With the doubly deprotonated ReC0A catalyst bound through bidentate linkages, passivating water molecules and

DOI: 10.1021/acs.jpcc.6b03165
J. Phys. Chem. C 2016, 120, 20970−20977

hydroxides were added to ensure neutrality. The catalyst, surface water molecules, and hydrogen-bonding hydroxide groups were allowed to relax at the density functional theory level using the ωb97xd hybrid functional,[41] the LANL2DZ[42] basis set for the Ti atoms, and the 6-31G(d) basis set[37,38] for all other atoms. This functional allows for the modeling of dispersion, which was utilized in modeling dimers. These optimizations were done using the Gaussian 09 program with its default optimization criteria and integration grid.[43]

Simulations of SFG spectra are based on calculations of ab initio derivatives of polarizabilities and dipole moments with respect to normal mode coordinates, as in our previous work.[44,45] In particular, $A_{q,\mathrm{eff}} = |\chi^{(2)}_{q,\mathrm{eff}}|$ is calculated for *ppp* spectra, obtained as depicted on Scheme 1, using *p*-polarized fields for the sum-frequency, incident visible, and incident infrared fields. Because of symmetry, the only nonzero components of the second-order susceptibility are χ_{xxz}, χ_{xzx}, χ_{zxx}, and χ_{zzz}.

The effective second-order susceptibilities are calculated as follows:[37]

$$\begin{aligned}\chi^{(2)}_{q,\mathrm{eff},ppp}(\gamma) = {} & -L_{xx}(\omega_{\mathrm{SFG}})L_{xx}(\omega_{\mathrm{Vis}})L_{zz}(\omega_{\mathrm{IR}})\cos(\alpha_{\mathrm{SFG}})\cos(\alpha_{\mathrm{Vis}})\sin(\alpha_{\mathrm{IR}})\chi^{(2)}_{xxz} \\ & - L_{xx}(\omega_{\mathrm{SFG}})L_{zz}(\omega_{\mathrm{Vis}})L_{xx}(\omega_{\mathrm{IR}})\cos(\alpha_{\mathrm{SFG}})\sin(\alpha_{\mathrm{Vis}})\cos(\alpha_{\mathrm{IR}})\chi^{(2)}_{xzx} \\ & + L_{zz}(\omega_{\mathrm{SFG}})L_{xx}(\omega_{\mathrm{Vis}})L_{xx}(\omega_{\mathrm{IR}})\sin(\alpha_{\mathrm{SFG}})\cos(\alpha_{\mathrm{Vis}})\cos(\alpha_{\mathrm{IR}})\chi^{(2)}_{zxx} \\ & + L_{zz}(\omega_{\mathrm{SFG}})L_{zz}(\omega_{\mathrm{Vis}})L_{zz}(\omega_{\mathrm{IR}})\sin(\alpha_{\mathrm{SFG}})\sin(\alpha_{\mathrm{Vis}})\sin(\alpha_{\mathrm{IR}})\chi^{(2)}_{zzz}\end{aligned} \tag{2}$$

where $\alpha_{\mathrm{VIS}} = 65°$ and $\alpha_{\mathrm{IR}} = 50°$ are the incident angles of the visible and IR fields, respectively, as described in section 2.2. The values of α_{SFG} are obtained as follows:

$$\alpha_{\mathrm{SFG}} = \arcsin\left(\frac{\omega_{\mathrm{Vis}}\sin\alpha_{\mathrm{Vis}} + \omega_{\mathrm{IR}}\sin\alpha_{\mathrm{IR}}}{\omega_{\mathrm{Vis}} + \omega_{\mathrm{IR}}}\right) = 63° \tag{3}$$

The Fresnel factors are computed as follows:

$$\begin{aligned}L_{xx}(\omega) &= \frac{2n_{\mathrm{air}}\cos(\arcsin(n_{\mathrm{air}}\sin\alpha_\omega/n_{\mathrm{TiO_2},\omega}))}{n_{\mathrm{air}}\cos(\arcsin(n_{\mathrm{air}}\sin\alpha_\omega/n_{\mathrm{TiO_2},\omega})) + n_{\mathrm{TiO_2},\omega}\cos\alpha_\omega} \\ L_{yy}(\omega) &= \frac{2n_{\mathrm{air}}\cos\alpha_\omega}{n_{\mathrm{air}}\cos\alpha_\omega + n_{\mathrm{TiO_2},\omega}\cos(\arcsin(n_{\mathrm{air}}\sin\alpha_\omega/n_{\mathrm{TiO_2},\omega}))} \\ L_{zz}(\omega) &= \frac{2n_{\mathrm{TiO_2},\omega}\cos\alpha_\omega}{n_{\mathrm{air}}\cos(\arcsin(n_{\mathrm{air}}\sin\alpha_\omega)/n_{\mathrm{TiO_2},\omega})) + n_{\mathrm{TiO_2},\omega}\cos\alpha_\omega} \\ &\quad \left(\frac{n_{\mathrm{air}}}{n_{\mathrm{interface},\omega}}\right)^2\end{aligned} \tag{4}$$

where $n_{\mathrm{TiO_2},\omega}$ is the index of refraction for the rutile TiO_2 surface, i.e., 2.56 (SFG), 2.52 (Vis), and 2.45 (IR, estimated value);[46,47] n_{air} the index of refraction for air, i.e., 1.00; and $n_{\mathrm{interface},\omega}$ the index of refraction for the resulting interface, 1.64 (SFG), 1.62 (Vis), and 1.59 (IR), which are calculated using the model reported by Zhuang et al.[37] ω as a subscript indicates a function of frequency, i.e., the IR, Vis, or SFG beam. Equation 2 then simplifies to

$$\begin{aligned}\chi^{(2)}_{\mathrm{eff},ppp}(\phi) = {} & -0.0608\chi^{(2)}_{xxz} - 0.0727\chi^{(2)}_{xzx} + 0.0705\chi^{(2)}_{zxx} \\ & + 0.0510\chi^{(2)}_{zzz}\end{aligned} \tag{5}$$

The second-order susceptibilities, $\chi^{(2)}_{ijk}$, are determined from the second-order hyperpolarizability elements, β_{abc}, as follows:

$$\chi^{(2)}_{ijk} = N_s \sum_{abc} R_{ia}R_{jb}R_{kc}\beta_{abc} \tag{6}$$

where N_s is the molecule number density and the rotation matrices transform the hyperpolarizability elements from the molecular coordinates frame (*a*,*b*,*c*) to the laboratory coordinate frame (*i*,*j*,*k*) = (*x*,*y*,*z*) through the Euler angles (θ,ψ,ϕ). The *ZXZ* rotation matrix formalism is used for all rotations, as described in eq 7.

$$R_{ia}R_{jb}R_{kc} = Z_\phi Z_\theta Z_\psi = \begin{pmatrix} -\sin\phi\cos\theta\sin\psi + \cos\phi\cos\psi & -\sin\phi\cos\theta\cos\psi - \cos\phi\sin\psi & \sin\phi\sin\theta \\ \cos\phi\cos\theta\cos\psi + \sin\phi\cos\psi & \cos\phi\cos\theta\cos\psi - \sin\phi\sin\psi & -\cos\phi\sin\theta \\ \sin\theta\sin\psi & \sin\theta\cos\psi & \cos\theta \end{pmatrix} \tag{7}$$

θ is the "tilt" angle between the molecular *c*-axis and the laboratory surface normal *z*-axis rotating counterclockwise around the [−110] axis. A more positive θ would result in the bipyridine plane bending toward the surface. ψ is the "twist" angle corresponding to the rotation of the molecular *a*-axis counterclockwise around the molecular *c*-axis following the θ angle rotation. With $\theta = 0°$, a more positive ψ results in rotation around the *z*-axis perpendicular to the TiO_2 surface. ϕ is the angle between the molecular *a*-axis and the [−110] axis rotating counterclockwise. To calculate the second-order susceptibility at different azimuthal orientations of TiO_2 crystal, the ϕ angle in eq 7 is modified to ϕ' ($\phi' = \phi + \gamma$).

The second-order hyperpolarizability elements are computed in terms of the ab initio derivatives of the polarizability and dipole moment with respect to normal mode coordinates Q as follows:[15,48]

$$\beta_{abc,q} = \frac{\partial\alpha_{ab}}{\partial Q_q}\frac{\partial\mu_c}{\partial Q_q} \tag{8}$$

For the SFG simulation, normal-mode analyses were performed for neutral gas phase ReC0A dimers in the absence of TiO_2, for the geometries of the dimer on the cluster, determined by optimization with the ωb97xd hybrid functional with dispersion.[41] Frequencies and hyperpolarizabilities, however, were computed by using the B3LYP hybrid functional[49−52] and the 6-311++G(d,p) basis set[53,54] because they correlate better with experiments. The "ultrafine" integration grid, which consists of 99 radial shells and 590 angular points per shell, was used. Dipole and polarizability derivatives for each vibrational mode were printed using the keyword "iop(7/33 = 1)" during the frequency calculations. All DFT calculations were performed using the Gaussian 09 program.[43] The normal-mode frequencies were scaled by 0.98. The definition of the orientation angles is

DOI: 10.1021/acs.jpcc.6b03165
J. Phys. Chem. C 2016, 120, 20970−20977

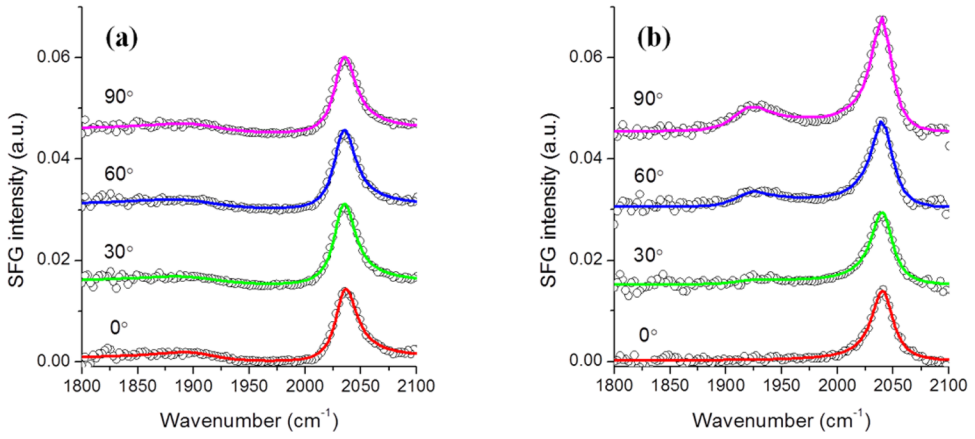

Figure 1. *ppp*-polarized SFG spectra of ReC0A on (a) TiO_2(001) and (b) TiO_2(110) in the carbonyl stretching region at azimuthal angles (γ) of 0°, 30°, 60°, and 90°. The open circles are SFG data, and the solid curves are fits according to eq 1.

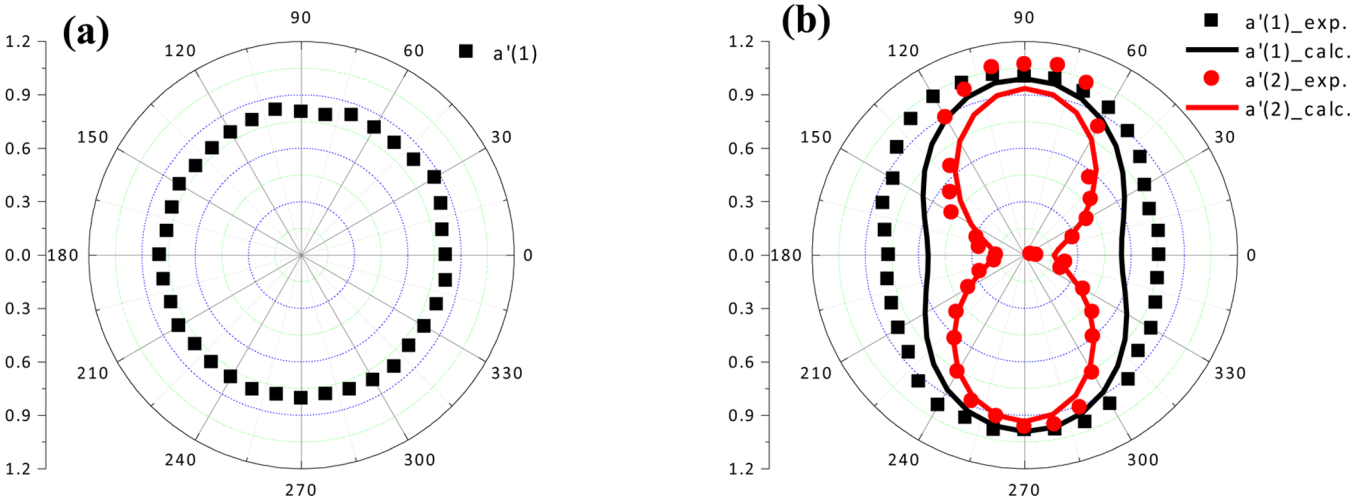

Figure 2. Polar plots of the azimuthal dependence of the amplitude for (a) the a′(1) mode of ReC0A on TiO_2(001) and (b) a′(1) and a′(2) modes of ReC0A on TiO_2(110). Black squares (a′(1)) and red circles (a′(2)) are experimental results; solid lines are calculated results. The amplitude of the a′(1) mode at γ = 90° for the ReC0A/TiO_2(110) system is normalized to one with all other data points for each mode scaled accordingly.

given in Scheme 1c and is discussed more in section 4 of the Supporting Information.

3. RESULTS AND DISCUSSION

3.1. Experimental Observations. Figure 1 shows the *ppp*-polarized SFG spectra of ReC0A on the TiO_2(001) and (110) surfaces in the carbonyl stretching region at azimuthal angles (γ) of 0°, 30°, 60°, and 90°. Here, γ is defined as the angle between the plane of the incident beams and the [001] and [−110] axes for the (001) and (110) surfaces, respectively. For ReC0A on the TiO_2(001) surface, the spectra showed no dependence on the azimuthal angle (Figure 1a). For ReC0A on the TiO_2(110) surface, the intensity of the peak at 2040 cm^{-1} gradually increased when the azimuthal angle increased from 0° to 90° (Figure 1b). Furthermore, a new band at ∼1920 cm^{-1} was observed to increase with azimuthal angle, reaching a maximum amplitude at γ = 90°. According to the IR results and our previous SFG results,[35,44] the higher-frequency bands at 2035 cm^{-1} in Figure 1a and at 2040 cm^{-1} in Figure 1b can be assigned to the in-phase symmetric mode of the three CO groups (a′(1) stretch); the lower-frequency band at ∼1920 cm^{-1} in Figure 1b can be assigned to the corresponding out-of-phase symmetric mode of the three CO groups (a′(2) stretch).

The IR spectra were measured for ReC0A on nanoporous TiO_2 thin films (Figures S2 and S3) to facilitate the assignment of SFG peaks. The IR spectrum of the full-coverage ReC0A sample exhibits three CO stretching bands: an in-phase symmetric a′(1) stretch centered at ∼2045 cm^{-1}, an antisymmetric a″ stretch at ∼1938 cm^{-1}, and an out-of-phase symmetric a′(2) stretch at ∼1917 cm^{-1}. As discussed in the Supporting Information, the peak positions blue-shift with the degree of coverage because of the formation of dimers and trimers.[55,56] The SFG results presented here correspond to the sample at saturated surface coverage.

The SFG spectrum at each azimuthal angle was fit according to eq 1. Figures 2a and 2b shows polar plots of the fitted effective amplitudes ($A_{q,\mathrm{eff}}$) of the symmetric CO stretch modes as a function of γ on the (001) and (110) surfaces. Experimental results with standard deviations are shown in Figure S4. ReC0A/TiO_2(001) shows no γ-dependence, as evidenced by its circular polar plot. ReC0A/TiO_2(110), however, shows a clear enhancement in SFG amplitude when the incident-light plane is along the [001] direction of TiO_2 for both a′(1) and a′(2) stretches. These results show that the structure of the ReC0A monolayer indeed reflects the effective C_{2v} symmetry of the TiO_2(110) surface. This also indicates that the isotropic distribution observed for the

DOI: 10.1021/acs.jpcc.6b03165
J. Phys. Chem. C 2016, 120, 20970−20977

ReC0A/TiO_2(001) system is most likely a direct result of the underlying (001) substrate symmetry (C_4).

3.2. Theoretical Determination of Binding Mode. We then examined the binding structures of ReC0A on the TiO_2(110) surface to understand the preferential alignment along the [−110] axis versus the [001] axis. In our previous studies, we found that bidentate binding modes are energetically favored.[35,44] Additionally, dissociated water molecules are known to form on the TiO_2(110) surface.[57−59] We relaxed the bidentate binding structures of ReC0A on a TiO_2(110) cluster passivated with water molecules using DFT methods as described in Computational Methods. The optimized bidentate binding mode along the [001] axis is labeled as **A** mode binding (Figure 3a), and the optimized binding along the [−110] axis is labeled as **B** mode binding (Figure 3b).

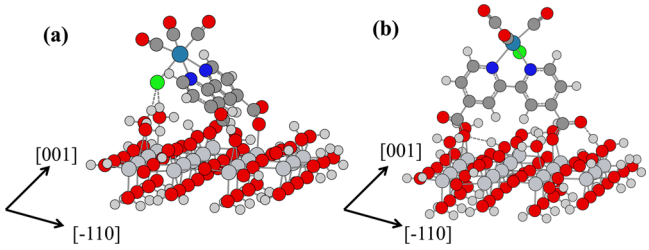

Figure 3. Binding structures of the ReC0A complex on the TiO_2(110) surface along the (a) [001] axis labeled as **A** mode binding and (b) [−110] axis labeled as **B** mode binding. Hydrogen bonding to the ReC0A complexes is depicted using single-dashed bonds. The atoms are colored as follows: green, Cl; silver, Ti; cerulean, Re; white, H; red, O; gray, C; and blue, N. The black arrows indicate the crystal axes on the surface for each panel.

We found that the **B** mode (Figure 3b) with a tilted bipyridine ring is the most energetically favorable, indicating that the ReC0A complex prefers to bind along the [−110] axis. Along this direction, the hydrogen bonding between the carboxylate group and the nearest OH group on the TiO_2 surface is aligned approximately within the π-conjugated plane of bipyridine and carboxylate, leading to a low-energy binding mode. In addition, there are four other OH groups hydrogen-bonding to the complex. In contrast, along the [001] direction (**A** mode in Figure 3a), the hydrogen bonding between the carboxylate group and the nearest OH group on the TiO_2 surface is aligned out of the π-conjugated plane of the bipyridine and carboxylate group. Also, four O−H hydrogen bonds have been replaced with two weak Cl−H hydrogen bonds. These interactions, or lack thereof, lead to a higher-internal-energy (by about 27 kcal/mol) binding mode. Therefore, the structural modeling indicates that the binding preference of ReC0A along the [−110] axis is associated with the nature of the TiO_2 atomic configuration and water on the TiO_2(110) surface.

3.3. Simulation of SFG Results. In the **B** mode, the tilt angle θ (the angle of the bpy ring plane relative to the surface) is about 13°. However, when modeled as a monomer, the computed SFG spectra of this optimized geometry do not match the measured one because the dipole derivative vector for the the a′(2) stretch would be nearly parallel to the surface (Figure S5) and has negligible SFG intensity. In addition, experimental evidence indicates that there is significant aggregation of ReC0A on the surface due to high surface coverage (see section 2 of the Supporting Information for details).[55,56] Therefore, "dimer" models were constructed in which each ReC0A is separately bound to the surface along the [−110] axis but are still close enough to each other to interact as nearest-neighbors, with all four combinations of axial ligand orientation relative to the surface (Figure 4 and Figure S6). As shown in Table S1, θ is

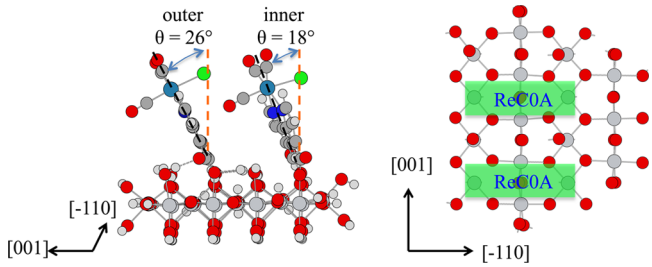

Figure 4. Binding structures of two ReC0A complexes as a dimer on the TiO_2(110) surface along the [−110] axis (**B** mode binding) from the side (left) and from above, omitting the ReC0A complexes with green rectangles indicating the binding sites of the two complexes (right). In both monomers, the CO ligand faces the surface. Hydrogen-bonding to the ReC0A complexes is depicted using single-dashed bonds. The atoms are colored as follows: green, Cl; silver, Ti; cerulean, Re; white, H; red, O; gray, C; and blue, N. The degree of tilt of each catalyst is indicated by the angle formed by the bpy ring (black dotted line) and the surface normal (orange dotted line), though the SFG spectra are generated from the molecular orientation as determined directly by whole dimer binding on the surface. The black arrows indicate the crystal directions on the surface for each panel.

significantly increased in all instances of this model to values ranging from 18° to 32°, which are bigger than the 13° tilt angle observed in the **B** mode. These configurations minimize the intermolecular steric interactions from the axial ligands of each ReC0A unit that would result if the bipyridine rings were parallel with each other.

To determine the ligand arrangement that is most consistent with the experiment results, we compared the measured and simulated[44] azimuthal angle dependence of the SFG signal. To determine the SFG spectra of each dimer model, the cluster was removed and the full frequencies and hyperpolarizabilities were then determined in the gas phase, as described in Computational Methods. The geometry changes induced by dimerization in these models are retained. These models take into account nearest-neighbor effects, which were found to be important in simulating the amide I stretch of proteins.[45] The theoretical azimuthal dependence of the effective SFG amplitudes for the a′(2) mode and the a′(1) mode are given as circular polar plots in Figure S6 for each of the four possible dimers as compared to the experimental spectra.

The comparison of the azimuthal dependence plots in Figure S6 shows that the best agreement between the measured and calculated amplitudes for modes that correspond to the a′(2) mode (1917 and 1925 cm^{-1}) and the a′(1) mode (2023 cm^{-1}) comes from the spectra for the entire dimer with the axial CO ligands facing the surface (structure I in Figure S6 and Tables S1 and S2). The geometry for this orientation is given in Figure 4 where the tilt angles are 26° and the 18° as defined by the diagram. Figure S7 shows that the agreement is improved with a slight tilt of 4° of the entire dimer relative to the surface normal, likely due to insufficient exploration of minima near the ones determined by DFT geometry optimizations.

The final polar plots shown in Figure 2b for the a′(2) mode were produced by averaging the contributions from the modes at 1917 cm^{-1} and at 1925 cm^{-1}. The a′(1) mode corresponds to the

DOI: 10.1021/acs.jpcc.6b03165
J. Phys. Chem. C 2016, 120, 20970−20977

2023 cm^{-1} band. The polar plots given in Figure S7 were averaged with that of equivalent twisted −20° about the surface normal to account for the C_2 symmetry of the (110) surface and therefore the direction of the axial CO ligands that determine the dipole and polarizability derivatives. The agreement between the theoretical and experimental polar plots (Figure 2b) indicates that the ReC0A molecules are bound as shown in Figure 4. This conclusion is corroborated by the energetic analysis given in Table S1, which shows that this structure has the minimum energy (−28.50 kcal/mol) relative to the structure with both Cl facing the surface (IV), when hydrogen bonding with the surface is accounted for. The other possibilities with exactly one Cl facing the surface have energies more positive than this reference.

We note that the rings here are not perfectly planar, especially in the case of the monomer with the Cl facing the center of the cluster, where the dihedral of the 5′ and 6′ C atoms is −13.7°. This kind of twisting is similar to that seen in the crystal structures of other Re(bpy) complexes,[60−63] especially in the case of [Re(bpy-*t*Bu)$(CO)_4$](OTf) where this dihedral angle is 8.2°.[60]

4. CONCLUSION

We have elucidated the arrangement of the rhenium bipyridyl catalyst (ReC0A) on different TiO_2 surfaces with distinct symmetries by combining vibrational SFG spectroscopy and DFT calculations of the SFG spectra. We find that ReC0A has a well-defined anisotropic arrangement on the TiO_2(110) surface, in contrast to the isotropic binding to the more symmetric TiO_2(001) surface. On the (110) surface, a maximum SFG intensity is observed when the incident light plane is aligned along the [001] axis. We find that the complex binds along the [−110] axis of TiO_2(110), stabilized by favorable hydrogen-bonding interactions between the carboxylate group and the water/OH groups on the TiO_2 surface. The binding mode of the ReC0A dimer, bound along the [−110] axis, with tilt angles of 18° and 26° (both carbonyls facing the surface), generates an average SFG spectrum that agrees with experimental measurements.

Overall, our study demonstrates the ability to prepare an electrocatalyst−semiconductor system with a preferred in-plane average molecular arrangement. The ability to control and characterize the molecular ordering and orientation through careful selection of the underlying substrate should be particularly valuable because the molecular orientation, relative to the electrode interface, can significantly affect the catalytic performance.

■ ASSOCIATED CONTENT

Supporting Information

The Supporting Information is available free of charge on the ACS Publications website at DOI: 10.1021/acs.jpcc.6b03165.

AFM image of TiO_2(110) single-crystal surface, FTIR spectra of ReC0A on TiO_2 nanoporous thin film, SFG spectra of ReC0A on TiO_2(001) surfaces, fitted amplitude values, electronic energies and theoretical SFG spectra for all ligand orientations of the dimer on TiO_2 along with dipole derivatives and displacement vectors for the stretches of the isolated monomer and for the dimer with both CO's facing the surface, additional references, and theoretical coordinates (PDF)

■ AUTHOR INFORMATION

Corresponding Authors

*Tel: (203) 432-6672. E-mail: victor.batista@yale.edu.
*Tel: (404) 727-6649. E-mail: tlian@emory.edu.

Present Addresses

⊥(D.X.) Department of Chemistry and Chemical Engineering, University of New Haven, West Haven, CT 06516.
#(C.L.A.) School of Science and Technology, Georgia Gwinnett College, Lawrenceville, GA 30043.

Author Contributions

‖A.G. and B.R. contributed equally to this work.

Notes

The authors declare no competing financial interest.

■ ACKNOWLEDGMENTS

This work was supported by Air Force Office of Scientific Research Grant FA9550-13-1-0020 (V.S.B. and T.L.). V.S.B. acknowledges high-performance computing time from NERSC and from the high-performance computing facilities at Yale. B.R. acknowledges support from the National Science Foundation Graduate Research Fellowship under Grant No. DGE-1122492. We thank Zheyuan Chen for help in AFM measurements, John Bacsa (Emory Crystallography Lab) for X-ray analyses of TiO_2 single crystals, and Melissa Clark and Cliff Kubiak (UC San Diego) for helpful discussions.

■ REFERENCES

(1) Underwood, A. J. V. Industrial Synthesis of Hydrocarbons from Hydrogen and Carbon Monoxide. *Ind. Eng. Chem.* **1940**, *32*, 449−454.
(2) Balazs, G. B.; Anson, F. C. Effects of CO on the Electrocatalytic Activity of Ni (cyclam)$^{2+}$ Toward the Reduction of CO_2. *J. Electroanal. Chem.* **1993**, *361*, 149−157.
(3) Raebiger, J. W.; Turner, J. W.; Noll, B. C.; Curtis, C. J.; Miedaner, A.; Cox, B.; DuBois, D. L. Electrochemical Reduction of CO_2 to CO Catalyzed by a Bimetallic Palladium Complex. *Organometallics* **2006**, *25*, 3345−3351.
(4) Benson, E. E.; Kubiak, C. P.; Sathrum, A. J.; Smieja, J. M. Electrocatalytic and Homogeneous Approaches to Conversion of CO_2 to Liquid Fuels. *Chem. Soc. Rev.* **2009**, *38*, 89−99.
(5) O'Toole, T. R.; Margerum, L. D.; Westmoreland, T. D.; Vining, W. J.; Murray, R. W.; Meyer, T. J. Electrocatalytic Reduction of CO_2 at a Chemically Modified Electrode. *J. Chem. Soc., Chem. Commun.* **1985**, 1416−1417.
(6) Yoshida, T.; Tsutsumida, K.; Teratani, S.; Yasufuku, K.; Kaneko, M. Electrocatalytic Reduction of CO_2 in Water by [Re(bpy)$(CO)_3$Br] and [Re(terpy)$(CO)_3$Br] Complexes Incorporated Into Coated Nafion Membrane (bpy = 2,2′-bipyridine; terpy = 2,2′:6′,2′′-terpyridine). *J. Chem. Soc., Chem. Commun.* **1993**, 631−633.
(7) Christensen, P.; Hamnett, A.; Muir, A. V. G.; Timney, J. A.; Higgins, S. Growth and Electrochemical Behaviour of a Poly [tricarbonyl(vinylbipyridyl)rhenium chloride] Film. Heterogeneous Reduction of CO_2. *J. Chem. Soc., Faraday Trans.* **1994**, *90*, 459−469.
(8) Adams, D. M.; Brus, L.; Chidsey, C. E. D.; Creager, S.; Creutz, C.; Kagan, C. R.; Kamat, P. V.; Lieberman, M.; Lindsay, S.; Marcus, R. A.; et al. Charge Transfer on the Nanoscale: Current Status. *J. Phys. Chem. B* **2003**, *107*, 6668−6697.
(9) Cecchet, F.; Alebbi, M.; Bignozzi, C. A.; Paolucci, F. Efficiency Enhancement of the Electrocatalytic Reduction of CO_2: *fac*-[Re(v-bpy)$(CO)_3$Cl] Electropolymerized onto Mesoporous TiO_2 Electrodes. *Inorg. Chim. Acta* **2006**, *359*, 3871−3874.
(10) Prezhdo, O. V.; Duncan, W. R.; Prezhdo, V. V. Dynamics of the Photoexcited Electron at the Chromophore-Semiconductor Interface. *Acc. Chem. Res.* **2008**, *41*, 339−348.
(11) Cheung, K. C.; Guo, P.; So, M. H.; Lee, L. Y. S.; Ho, K. P.; Wong, W. L.; Lee, K. H.; Wong, W. T.; Zhou, Z. Y.; Wong, K. Y. Electrocatalytic

DOI: 10.1021/acs.jpcc.6b03165
J. Phys. Chem. C 2016, 120, 20970−20977

Reduction of Carbon Dioxide by a Polymeric Film of Rhenium Tricarbonyl Dipyridylamine. *J. Organomet. Chem.* **2009**, *694*, 2842−2845.
(12) Chen, Z.; Shen, Y.; Somorjai, G. A. Studies of Polymer Surfaces by Sum Frequency Generation Vibrational Spectroscopy. *Annu. Rev. Phys. Chem.* **2002**, *53*, 437−465.
(13) Shen, Y. Phase-Sensitive Sum-Frequency Spectroscopy. *Annu. Rev. Phys. Chem.* **2013**, *64*, 129−150.
(14) Wang, H.-F.; Velarde, L.; Gan, W.; Fu, L. Quantitative Sum-Frequency Generation Vibrational Spectroscopy of Molecular Surfaces and Interfaces: Lineshape, Polarization, and Orientation. *Annu. Rev. Phys. Chem.* **2015**, *66*, 189−216.
(15) Shen, Y. R. *The Principles of Nonlinear Optics*; J. Wiley: New York, 1984; pp *xii*, 563.
(16) Rich, C. C.; Mattson, M. A.; Krummel, A. T. Direct Measurement of the Absolute Orientation of N3 Dye at Gold and Titanium Dioxide Surfaces with Heterodyne-Detected Vibrational SFG Spectroscopy. *J. Phys. Chem. C* **2016**, *120*, 6601−6611.
(17) Clark, M. L.; Rudshteyn, B.; Ge, A.; Chabolla, S. A.; Machan, C. W.; Psciuk, B. T.; Song, J.; Canzi, G.; Lian, T.; Batista, V. S.; Kubiak, C. P. Orientation of Cyano-Substituted Bipyridine Re(I) *fac*-Tricarbonyl Electrocatalysts Bound to Conducting Au Surfaces. *J. Phys. Chem. C* **2016**, *120*, 1657.
(18) Wang, J.; Clark, M. L.; Li, Y.; Kaslan, C. L.; Kubiak, C. P.; Xiong, W. Short-Range Catalyst−Surface Interactions Revealed by Heterodyne Two-Dimensional Sum Frequency Generation Spectroscopy. *J. Phys. Chem. Lett.* **2015**, *6*, 4204−4209.
(19) Calabrese, C.; Vanselous, H.; Petersen, P. B. Deconstructing the Heterogeneity of Surface-Bound Catalysts: Rutile Surface Structure Affects Molecular Properties. *J. Phys. Chem. C* **2016**, *120*, 1515−1522.
(20) Kim, D.; Oh-e, M.; Shen, Y. R. Rubbed Polyimide Surface Studied by Sum-Frequency Vibrational Spectroscopy. *Macromolecules* **2001**, *34*, 9125−9129.
(21) Oh-e, M.; Kim, D.; Shen, Y. R. Surface Anisotropy from Photo-Induced Bond Breaking at Polymer Surfaces: A Sum-Frequency Vibrational Spectroscopic Study of Polyimide. *J. Chem. Phys.* **2001**, *115*, 5582−5588.
(22) Jayathilake, H. D.; Zhu, M. H.; Rosenblatt, C.; Bordenyuk, A. N.; Weeraman, C.; Benderskii, A. V. Rubbing-Induced Anisotropy of Long Alkyl Side Chains at Polyimide Surfaces. *J. Chem. Phys.* **2006**, *125*, 064706.
(23) Sung, J.; Waychunas, G. A.; Shen, Y. R. Surface-Induced Anisotropic Orientations of Interfacial Ethanol Molecules at Air/Sapphire($1\bar{1}02$) and Ethanol/Sapphire($1\bar{1}02$) Interfaces. *J. Phys. Chem. Lett.* **2011**, *2*, 1831−1835.
(24) Sung, J. H.; Zhang, L. N.; Tian, C. S.; Waychunas, G. A.; Shen, Y. R. Surface Structure of Protonated R-Sapphire ($1\bar{1}02$) Studied by Sum-Frequency Vibrational Spectroscopy. *J. Am. Chem. Soc.* **2011**, *133*, 3846−3853.
(25) Jang, J. H.; Lydiatt, F.; Lindsay, R.; Baldelli, S. Quantitative Orientation Analysis by Sum Frequency Generation in the Presence of Near-Resonant Background Signal: Acetonitrile on Rutile TiO_2 (110). *J. Phys. Chem. A* **2013**, *117*, 6288−6302.
(26) Tong, Y.; Wirth, J.; Kirsch, H.; Wolf, M.; Saalfrank, P.; Campen, R. K. Optically Probing Al—O and O—H Vibrations to Characterize Water Adsorption and Surface Reconstruction on α-Alumina: An Experimental and Theoretical Study. *J. Chem. Phys.* **2015**, *142*, 054704.
(27) Hawecker, J.; Lehn, J. M.; Ziessel, R. Electrocatalytic Reduction of Carbon Dioxide Mediated by Re(bipy)$(CO)_3$Cl (bipy = 2,2′-Bipyridine). *J. Chem. Soc., Chem. Commun.* **1984**, 328−330.
(28) Hawecker, J.; Lehn, J. M.; Ziessel, R. Photochemical and Electrochemical Reduction of Carbon Dioxide to Carbon Monoxide Mediated by (2,2′-Bipyridine)tricarbonylchlororhenium(I) and Related Complexes as Homogeneous Catalysts. *Helv. Chim. Acta* **1986**, *69*, 1990−2012.
(29) Juris, A.; Campagna, S.; Bidd, I.; Lehn, J. M.; Ziessel, R. Synthesis and Photophysical and Electrochemical Properties of New Halotricarbonyl(Polypyridine)Rhenium(I) Complexes. *Inorg. Chem.* **1988**, *27*, 4007−4011.
(30) Yam, V. W. W.; Lau, V. C. Y.; Cheung, K. K. Synthesis and Photophysics of Luminescent Rhenium(I) Acetylides-Precursors for Organometallic Rigid-Rod Materials - X-Ray Crystal-Structures of [Re(^{t}Bu$_2$)$(CO)_3$(^{t}BuC ≡ C)] and [Re(^{t}Bu$_2$bpy)$(CO)_3$Cl]. *Organometallics* **1995**, *14*, 2749−2753.
(31) Hayashi, Y.; Kita, S.; Brunschwig, B. S.; Fujita, E. Involvement of a Binuclear Species with the Re−C(O)O−Re Moiety in CO_2 Reduction Catalyzed by Tricarbonyl Rhenium(I) Complexes with Diimine Ligands: Strikingly Slow Formation of the Re−Re and Re−C(O)O−Re Species from Re(dmb) $(CO)_3$S (dmb = 4,4′-Dimethyl-2,2′-bipyridine, S = Solvent). *J. Am. Chem. Soc.* **2003**, *125*, 11976−11987.
(32) Fujita, E.; Muckerman, J. T. Why Is Re-Re Bond Formation/Cleavage in $[Re(bpy)\ (CO)_3]_2$ Different from That in $[Re(CO)_5]_2$? Experimental and Theoretical Studies on the Dimers and Fragments. *Inorg. Chem.* **2004**, *43*, 7636−7647.
(33) Takeda, H.; Koike, K.; Inoue, H.; Ishitani, O. Development of an Efficient Photocatalytic System for CO_2 Reduction Using Rhenium(L) Complexes Based on Mechanistic Studies. *J. Am. Chem. Soc.* **2008**, *130*, 2023−2031.
(34) Smieja, J. M.; Kubiak, C. P. Re(bipy-tBu)$(CO)_3$Cl−improved Catalytic Activity for Reduction of Carbon Dioxide: IR-Spectroelectrochemical and Mechanistic Studies. *Inorg. Chem.* **2010**, *49*, 9283−9289.
(35) Anfuso, C. L.; Snoeberger, R. C., III; Ricks, A. M.; Liu, W.; Xiao, D.; Batista, V. S.; Lian, T. Covalent Attachment of a Rhenium Bipyridyl CO_2 Reduction Catalyst to Rutile TiO_2. *J. Am. Chem. Soc.* **2011**, *133*, 6922−6925.
(36) Spitler, M. T.; Parkinson, B. A. Dye Sensitization of Single Crystal Semiconductor Electrodes. *Acc. Chem. Res.* **2009**, *42*, 2017−2029.
(37) Zhuang, X.; Miranda, P. B.; Kim, D.; Shen, Y. R. Mapping Molecular Orientation and Conformation at Interfaces by Surface Nonlinear Optics. *Phys. Rev. B: Condens. Matter Mater. Phys.* **1999**, *59*, 12632−12640.
(38) Soler, J. M.; Artacho, E.; Gale, J. D.; Garcia, A.; Junquera, J.; Ordejon, P.; Sanchez-Portal, D. The SIESTA Method for ab Initio Order-*N* Materials Simulation. *J. Phys.: Condens. Matter* **2002**, *14*, 2745−2779.
(39) Perdew, J. P.; Burke, K.; Ernzerhof, M. Generalized Gradient Approximation Made Simple. *Phys. Rev. Lett.* **1996**, *77*, 3865−3868.
(40) Perdew, J. P.; Burke, K.; Ernzerhof, M. Generalized Gradient Approximation Made Simple (vol 77, pg 3865, 1996). *Phys. Rev. Lett.* **1997**, *78*, 1396−1396.
(41) Chai, J.-D.; Head-Gordon, M. Long-Range Corrected Hybrid Density Functionals with Damped Atom-Atom Dispersion Corrections. *Phys. Chem. Chem. Phys.* **2008**, *10*, 6615−6620.
(42) Hay, P. J.; Wadt, W. R. Ab Initio Effective Core Potentials for Molecular Calculations. Potentials for K to Au Including the Outermost Core Orbitals. *J. Chem. Phys.* **1985**, *82*, 299−310.
(43) Frisch, M. J.; Trucks, G. W.; Schlegel, H. B.; Scuseria, G. E.; Robb, M. A.; Cheeseman, J. R.; Scalmani, G.; Barone, V.; Mennucci, B.; Petersson, G. A. et al. *Gaussian 09*, revision D.01; Gaussian, Inc.: Wallingford, CT, 2013.
(44) Anfuso, C. L.; Xiao, D.; Ricks, A. M.; Negre, C. F. A.; Batista, V. S.; Lian, T. Orientation of a Series of CO_2 Reduction Catalysts on Single Crystal TiO_2 Probed by Phase-Sensitive Vibrational Sum Frequency Generation Spectroscopy (PS-VSFG). *J. Phys. Chem. C* **2012**, *116*, 24107−24114.
(45) Xiao, D.; Fu, L.; Liu, J.; Batista, V. S.; Yan, E. C. Y. Amphiphilic Adsorption of Human Islet Amyloid Polypeptide Aggregates to Lipid/Aqueous Interfaces. *J. Mol. Biol.* **2012**, *421*, 537−547.
(46) Rams, J.; Tejeda, A.; Cabrera, J. Refractive Indices of Rutile as a Function of Temperature and Wavelength. *J. Appl. Phys.* **1997**, *82*, 994−997.
(47) DeVore, J. R. Refractive Indices of Rutile and Sphalerite. *J. Opt. Soc. Am.* **1951**, *41*, 416−419.
(48) Moad, A. J.; Simpson, G. J. A Unified Treatment of Selection Rules and Symmetry Relations for Sum-Frequency and Second Harmonic Spectroscopies. *J. Phys. Chem. B* **2004**, *108*, 3548−3562.

DOI: 10.1021/acs.jpcc.6b03165
J. Phys. Chem. C 2016, 120, 20970−20977

(49) Vosko, S. H.; Wilk, L.; Nusair, M. Accurate Spin-Dependent Electron Liquid Correlation Energies for Local Spin Density Calculations: A Critical Analysis. *Can. J. Phys.* **1980**, *58*, 1200−1211.
(50) Lee, C. T.; Yang, W. T.; Parr, R. G. Development of the Colle-Salvetti Correlation-Energy Formula Into a Functional of the Electron Density. *Phys. Rev. B: Condens. Matter Mater. Phys.* **1988**, *37*, 785−789.
(51) Becke, A. D. Density-Functional Thermochemistry. III. The Role of Exact Exchange. *J. Chem. Phys.* **1993**, *98*, 5648−5652.
(52) Stephens, P. J.; Devlin, F. J.; Chabalowski, C. F.; Frisch, M. J. Ab Initio Calculation of Vibrational Absorption and Circular Dichroism Spectra Using Density Functional Force Fields. *J. Phys. Chem.* **1994**, *98*, 11623−11627.
(53) Krishnan, R.; Binkley, J. S.; Seeger, R.; Pople, J. A. Self-Consistent Molecular Orbital Methods. XX. A Basis Set for Correlated Wave Functions. *J. Chem. Phys.* **1980**, *72*, 650−654.
(54) McLean, A. D.; Chandler, G. S. Contracted Gaussian Basis Sets for Molecular Calculations. I. Second Row Atoms, Z = 11−18. *J. Chem. Phys.* **1980**, *72*, 5639−5648.
(55) Laaser, J. E.; Christianson, J. R.; Oudenhoven, T. A.; Joo, Y.; Gopalan, P.; Schmidt, J.; Zanni, M. T. Dye Self-Association Identified by Intermolecular Couplings Between Vibrational Modes as Revealed by Infrared Spectroscopy, and Implications for Electron Injection. *J. Phys. Chem. C* **2014**, *118*, 5854−5861.
(56) Oudenhoven, T. A.; Joo, Y.; Laaser, J. E.; Gopalan, P.; Zanni, M. T. Dye Aggregation Identified by Vibrational Coupling Using 2D IR Spectroscopy. *J. Chem. Phys.* **2015**, *142*, 212449.
(57) Griffiths, D. M.; Rochester, C. H. Infrared Study of the Adsorption of Water on to the Surface of Rutile. *J. Chem. Soc., Faraday Trans. 1* **1977**, *73*, 1510−1529.
(58) Walle, L. E.; Borg, A.; Uvdal, P.; Sandell, A. Experimental Evidence for Mixed Dissociative and Molecular Adsorption of Water on a Rutile TiO_2(110) Surface Without Oxygen Vacancies. *Phys. Rev. B: Condens. Matter Mater. Phys.* **2009**, *80*, 235436.
(59) Sun, C. H.; Liu, L. M.; Selloni, A.; Lu, G. Q.; Smith, S. C. Titania-Water Interactions: A Review of Theoretical Studies. *J. Mater. Chem.* **2010**, *20*, 10319−10334.
(60) Grice, K. A.; Gu, N. X.; Sampson, M. D.; Kubiak, C. P. Carbon Monoxide Release Catalysed by Electron Transfer: Electrochemical and Spectroscopic Investigations of [Re(bpy-R)$(CO)_4$](OTf) Complexes Relevant to CO_2 Reduction. *Dalton Trans.* **2013**, *42*, 8498−8503.
(61) Chabolla, S. A.; Dellamary, E. A.; Machan, C. W.; Tezcan, F. A.; Kubiak, C. P. Combined Steric and Electronic Effects of Positional Substitution on Dimethyl-Bipyridine Rhenium(I)tricarbonyl Electrocatalysts for the Reduction of CO_2. *Inorg. Chim. Acta* **2014**, *422*, 109−113.
(62) Benson, E. E.; Kubiak, C. P. Structural Investigations into the Deactivation Pathway of the CO_2 Reduction Electrocatalyst Re(bpy)$(CO)_3$Cl. *Chem. Commun.* **2012**, *48*, 7374−7376.
(63) Benson, E. E.; Grice, K. A.; Smieja, J. M.; Kubiak, C. P. Structural and Spectroscopic Studies of Reduced [Re(bpy-R)$(CO)_3]^{-1}$ Species Relevant to CO_2 Reduction. *Polyhedron* **2013**, *58*, 229−234.

DOI: 10.1021/acs.jpcc.6b03165
J. Phys. Chem. C 2016, 120, 20970−20977